Article

pubs.acs.org/Biomac

Synthesis and Characterization of Water-Soluble Silk Peptides and Recombinant Silk Protein Containing Polyalanine, the Integrin Binding Site, and Two Glutamic Acids at Each Terminal Site as a Possible Candidate for Use in Bone Repair Materials

Tetsuo Asakura,*[,†] Yu Suzuki,[†] Aya Nagano,[†] David Knight,[‡] Masakatsu Kamiya,[§] and Makoto Demura[§]

[†]Department of Biotechnology, Tokyo University of Agriculture and Technology, Koganei, Tokyo 184-8588, Japan

[‡]Oxford Biomaterials, Ltd., Magdalen Centre, Oxford, OX4 4GA, United Kingdom

[§]Graduate School of Life Science, Hokkaido University, Sapporo, 060-0810, Japan

ABSTRACT: The recombinant proteins $[EE(A)_{12}EETGRGDSPAAS]_n$ (n = 5,10) were prepared as a potential scaffold material for bone repair. The construct was based on *Antheraea perni* silk fibroin to which cells adhere well and combined poly(alanine), the integrin binding site TGRGDSPA, and a pair of glutamic acids (E_2) at both the N- and C-terminal sites to render the construct water-soluble and with the hope that it might enhance mineralization with hydroxyapatite. Initially, two peptides $E_2(A)_nE_2TGRGDSPAE_2(A)_nE_2$ (n = 6, 12) were prepared by solid state synthesis to examine the effect of size on conformation and on cell binding. The larger peptide bound osteoblasts more readily and had a higher helix content than the smaller one. Titration of the side chain COO^- to COOH of the E_2 and D units in the peptide was monitored by solution NMR. On the basis of these results, we produced the related recombinant *His* tagged protein $[EE(A)_{12}EETGRGDSPAAS]_n$ (n = 5,10) by expression in *Escherichia coli*. The solution NMR spectra of the recombinant protein indicated that the poly(alanine) regions are helical, and one E_2 unit is helical and the other is a random coil. A molecular dynamics simulation of the protein supports these conclusions from NMR. We showed that the recombinant protein, especially, $[EE(A)_{12}EETGRGDSPAAS]_{10}$ has some of the properties required for bone tissue engineering scaffold including insolubility, and evidence of enhanced cell binding through focal adhesions, and enhanced osteogenic expression of osteoblast-like cells bound to it, and has potential for use as a bone repair material.

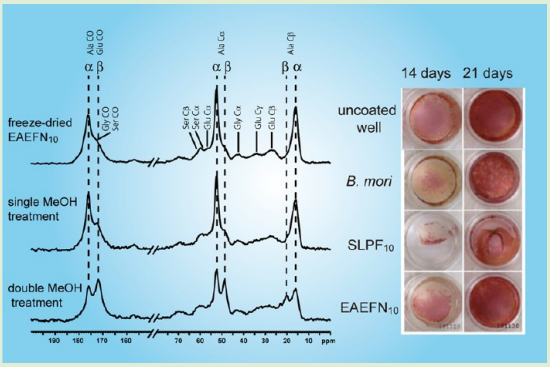

INTRODUCTION

Silks are generally defined as fibrous proteins that are spun into fibers by arthropods including spiders, lepidopteran larvae, hymenopterans, scorpions, and mites.[1] They have many advantageous properties as biomaterials, including strength, toughness, resilience, biocompatibility, and biodegradability.[2−11] In addition, aqueous solutions prepared from redissolved silks can be used to form fibers, films, powders, gels and sponges, with a wide range of potential biomedical applications.[3−5,10−12] Silk fibroin from the domesticated Mulberry silkworm, *Bombyx mori*, has been widely used for these purposes. In addition, there are a large number of wild silkworm species from different families that produce silk fibroins with a wide range of primary and higher ordered structures and properties.[1] Among these, the entire primary structure of *Antheraea pernyi* fibroin has been determined[13] and contains polyalanine (poly(Ala)) and Gly-rich domains. Some silk fibroins contain the arginine-glycine-aspartic acid triplet (RGD), which is present in the cell adhesive sequence found in fibronectin.[13,14] In this connection, Minoura et al.[15,16] showed that fibroin films prepared from *A. pernyi* silk had good cell adhesion and may have potential for use in bone repair.

The structure and structural transition of *A. pernyi* silk fibroin in the solid state has been studied with ^{13}C CP/MAS NMR in detail.[17] The conformation-dependent ^{13}C NMR chemical shift of the silk fibroin was very useful because the chemical shift of each carbon of the individual residues in the ^{13}C NMR spectrum changes depending on the conformation and conformational transition. Thus, ^{13}C CP/MAS NMR can be used for structural determination in model silk peptides, silk fibroin itself, and recombinant silk-like proteins through information on the local electronic state and local conformation in the forms of powders, films, and fibers rather than the single crystals required for detailed local conformational studies using X-ray or synchrotron diffraction.

In the present paper, we report the development of a novel recombinant silk-like protein that mimics *A. pernyi* silk fibroin. The most striking characteristic of this silk fibroin is the combination of poly(Ala) domains and multiple copies of the TGRGDSPA. The latter sequence is found in the cell adhesive

Received: July 28, 2013
Revised: August 26, 2013
Published: September 4, 2013

Figure 1. The designed oligonucleotide sequences for P2.

protein, fibronectin, but not in native *A. pernyi* fibroin. It has been previously shown that introduction of this sequence into a fibroin-mimetic protein results in greater cell-adhesion compared with introduction of the triplet RGD on its own without the flanking TGR and SPA sequences.[18−20] In designing the new construct, we also took into consideration the length of the $(Ala)_n$ domain and the effect of this highly hydrophobic sequence on the solubility of recombinant silk-like proteins. When n in this domain is 12, the most frequent length in natural *A. pernyi* silk fibroin, the poly(Ala) is insoluble in water.[17] However, the introduction of glutamic acids at the N- and C-terminal sites of poly(Ala) renders the construct water-soluble.[21−24] An additional potential advantage of the inclusion of pairs of glutamic acid residues is that polyglutamic acid is known to nucleate hydroxyapatite formation in several proteins.[25]

Therefore we initially used solid state synthesis to produce peptides $E_2(A)_nE_2TGRGDSPA\text{-}E_2(A)_nE_2$ with n = 6 (P1) or n = 12 (P2) to examine the effect of poly(Ala) length on the cell adhesive activity and the solution structure. Thereafter, the silk-like protein $[E_2(A)_{12}E_2TGRGDSPAAS]_5$ (hereafter abbreviated as$EAEFN_5$) and $EAEFN_{10}$ were produced by expression in *Escherichia coli*. The CD and solution NMR were used to study the structure of both the silk-like peptides and the recombinant proteins. An MD simulation was also performed for the sequence of the protein to confirm the NMR results. However, the protein $EAEFN_5$ was still soluble in water after methanol treatment, so it could not be used to coat the surface of wells used for direct cell binding assays. Therefore we expressed the larger construct $EAEFN_{10}$ in *E. coli*, which proved to soluble in water, but insoluble after methanol treatment. The ability of coatings of this construct to promote osteoblast cell adhesion activity was assessed using an assay based on the adhesion, flattening and development of focal adhesions of a mouse osteoblast-like cell line MC3T3-E1. The construct's ability to promote cell adhesion was compared with that of *B. mori* silk fibroin and another recombinant silk-like protein, $TS\text{-}(TGRGDSPAGG(GAGAGS)_3AS)_{10}$, $SLPF_{10}$ having the combination of the sequence, $(GAGAGS)_n$ in the crystalline domain of *B. mori* silk fibroin and multiple copies of the TGRGDSPA prepared in our laboratory previously.[26] Osteoblastic mineralization was also evaluated by Arizarin red staining after 14 and 21 days culture of MC3T3-E1 on coatings of $EAEFN_{10}$, and compared with those of *B. mori* silk fibroin and $SLPF_{10}$. Conformation-dependent chemical shifts in ^{13}C CP/MAS NMR spectra of $EAEFN_{10}$ were used to monitor methanol-induced structural change from the water-soluble film to the water-insoluble one. Thus, we synthesized and characterized the structure of water-soluble silk peptides and recombinant silk protein containing polyalanine, the integrin binding site and two glutamic acids at each terminal site to carry out an initial evaluation of some properties of these constructs relevant to their potential use in bone scaffolds.

MATERIALS AND METHODS

1. Preparation of Peptides. The Fmoc solid-phase method using a fully automated Pioneer Peptide Synthesis System (Applied Biosystems Ltd. Japan) was used to prepare two peptides, $E_2(A)_6E_2TGRGDSPAE_2(A)_6E_2$ (P1) and $E_2(A)_{12}E_2TGRGDSPAE_2(A)_{12}E_2$ (P2) to test the effect of the length of the poly(Ala) repeat. The crude peptides were purified by RP-HPLC using acetonitrile/0.1% trifluoroacetic acid (TFA) elution. After purification, acetonitrile was removed by evaporation, and then aqueous solutions of the peptides were lyophilized for 24 h.

2. Preparation of Recombinant Silk-like Proteins, $[E_2(A)_{12}E_2\text{-}TGRGDSPAAS]_n$ (n = 5, 10). The general method for the production of the recombinant silk-like protein has been described elsewhere.[18,19,26,27] The monomeric DNA duplex ligated into pUC57 was shown in Figure 1. The DNA sequence was designed as follows. The DNA fragment encoded a hybrid protein consisting of a poly(Ala) region derived from *A. pernyi* silk fibroin and a cell adhesive sequence from fibronectin, together with 5′-NheI and 3′-SpeI termini. Since base composition and sequence of the DNA can influence the polypeptide expression level and the stability of the DNA itself, codons with the highest A-T content were used. To construct the multimers, the plasmid pUC57 containing the monomer (or multimers) was digested with NotI and NheI, generating a linear vector containing the monomer (or multimer) insert. Another insert-containing plasmid was digested with NotI and SpeI, liberating the insert DNA fragment. The linearized vectors and insert DNA fragments obtained as above were extracted separately from the agarose slice and then the two were ligated. This process was repeated to the desired degree of polymerization of the DNA fragment unit. For expression, the insert was excised from pUC57-multimer by NotI and *Hin*dIII digestion, subcloned directly into pPAL7 (Bio-Rad Laboratories, Inc.) and transformed into BL21(DE3)pLysS. Larger-scale cell cultivation was performed using a fermenter (Marubishi Bio Eng. Japan), and expression was induced with IPTG. The production was checked by western-blotting. The silk-like proteins were purified with Profinity eXact fusion-tag chromatography system, followed by SDS-PAGE to identify the expression of hybrid proteins. The plasmids pUC57 and pPAL7 were purchased from Hokkaido System Science Co., Ltd. (Sapporo, Japan) and Bio-Rad Laboratories, Inc. respectively. *E. coli* DH5α was used for propagation and construction of plasmids, and BL21(DE3)pLysS was used for the expression of proteins. The synthesis of the oligonucleotides designed in this study was performed by Hokkaido System Science Co., Ltd. Restriction and ligase enzymes were purchased from Takara Bio Inc.(Shiga, Japan). Two His-tagged recombinant silk-like proteins with sequences, $SLPF_{10}$ and $(TGRGDSPAAS)_8$, respectively, were prepared in our laboratory as described elsewhere.[26,27] The former protein contains the sequence $AGG(GAGAGS)_n$ seen in the consensus sequence of *B. mori* fibroin together with the integrin binding motif of fibronectin, while the latter protein was used to compare osteoblast adhesion to $EAEFN_n$ (where n = 5,10) with that of these two other RGD-containing constructs previously investigated in our laboratory.[26,27] The pI values of three proteins, $EAEFN_n$ (n = 5, 10) and $SFPF_{10}$ were calculated to be 3.79, 3.77, and 5.97, respectively.

3. CD Measurements. CD spectra were recorded on a Jasco J-805 spectrometer (JASCO, Japan) using a 1 mm path-length cell at room temperature. The measurements were carried out in the wavelength range between 185 and 260 nm. The concentrations of two peptides, P1 and P2, and $EAEFN_n$ (where n = 5, 10) were 0.01% (wt/v) in H_2O.

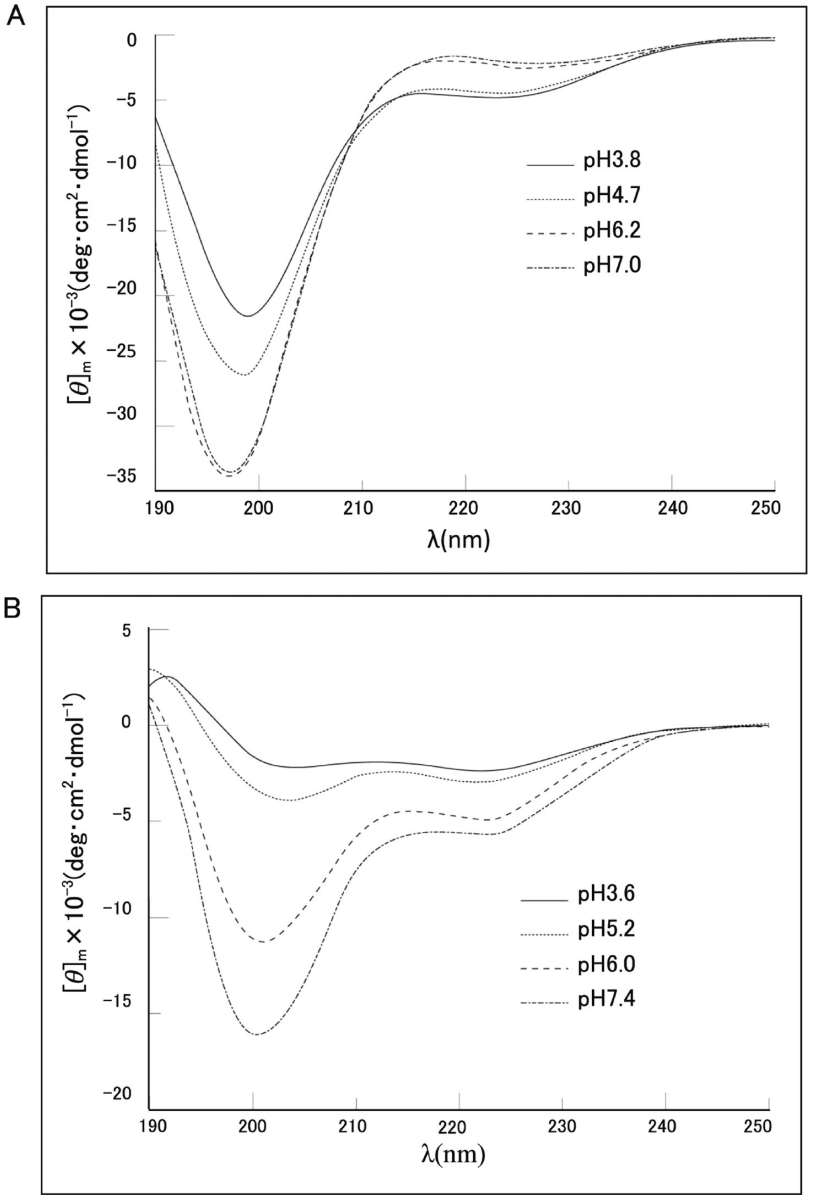

Figure 2. CD spectra of P1 (A) and P2 (B) in aqueous solutions as a function of pH.

The pH of the solutions was adjusted by the addition of small quantities of dilute HCl or NaOH solutions.

4. Solution NMR Measurement. For solution NMR analysis, uniformly ^{15}N- and ^{13}C/^{15}N-labeled protein, EAEFN$_5$ was expressed as His-tagged protein from *E. coli* in ^{15}N-rich or both ^{15}N- and ^{13}C-rich CHL medium (Shoko Co., Ltd. Japan). The protein solutions were concentrated to 0.3−0.5 mM with an Amicon Ultra device (Millipore, Bedford, MA). The NMR samples contained a final concentration of 50 mM sodium phosphate solution, 1 mM dithiothreitol (DTT), 50 μM 2,2-dimethyl-2-silapentane-5-sulfonate sodium salt and 10% D_2O. ^{1}H−^{13}C HSQC and TOCSY were acquired at 20 °C on a Bruker DMX-500 spectrometer. The obtained NMR data were processed with NMR Pipe[28] and analyzed with Sparky software. The pH of the solutions was adjusted to pH 4.0 and pH 7.0. The peptide, P2, in aqueous solution was also used for solution NMR observation under the same conditions.

5. Solid State NMR Measurement. The EAEFN$_{10}$ sample after freeze-drying was soluble in water. Repeated dipping in 90% methanol was used to render films of the construct insoluble .The ^{13}C CP/MAS NMR spectra of EAEFN$_{10}$ sample before and after methanol treatments were obtained on a Bruker DSX-400 AVANCE spectrometer with an operating frequency of 100.0 MHz for ^{13}C at a sample spinning rate of 8 kHz in a 4 mm diameter ZrO_2 rotor. A total of 7−20 K scans were collected over a spectral width of 25 kHz with a recycle delay of 5s. All spectra were obtained using a cross-polarization time of 1.5 ms, and broad-band proton decoupling. Phase cycling was used to minimize artifacts. ^{13}C chemical shifts were represented relative to those of tetramethylsilane (TMS).

6. Molecular Dynamics (MD) Simulation. We performed an MD simulation of the protein TS(EAEFN$_5$) with the sequence TS[E$_2$(A)$_{12}$E$_2$TGRGDSPAAS]$_2$E$_2$(A)$_{12}$E$_2$TGRGDSPAAS[E$_2$(A)$_{12}$E$_2$-TGRGDSPAAS]$_2$, which is basically identical to EAEFN$_5$ but with the addition of N-terminus TS. In the simulation, 100 chains of TS(EAEFN$_5$) surrounded by water molecules were generated with the Amber option, solvate box TIP3PBOX under periodic boundary conditions. As a starting point, the random coil conformation of TS(EAEFN$_5$) was generated by the Monte Carlo chain growth method[29] and then solvated. All of the simulations were performed using ff03 force field with 200 000 steps at 25 °C. The difference in the helix content before and after MD simulation was plotted against the number of the residue. The helical region was assumed to be $\phi = -64° \pm 15°$ and $\varphi = -41° \pm 15°$ in the Ramachandran map.[24]

7. Cell Adhesion Assay. Methanol-treated coatings of EAEFN$_{10}$ were used for the cell adhesion and osteogenic expression assay. For

comparison, coatings of another silk-like protein, $SLPF_{10}$ prepared in our group previously[26,27] was also used together with the coatings prepared from *B. mori* silk fibroin. The wells of 96-well tissue culture plates (0.33 cm^2/wells, Falcon U.K.) were coated with regenerated *B. mori* silk fibroin or $EAEFN_{10}$ or $SLPF_{10}$ (all at 50 $\mu g/cm^2$), and the coatings were rendered insoluble by repeatedly filling the wells with 90% methanol over a period of 30 min. Noncoated wells were used as standard. The ability of the surfaces to promote osteoblast cell adhesion activity of each protein was tested using mouse osteoblast-like cell line MC3T3-E1 cells.[30] MC3T3-E1 cells obtained from Riken were added to each well to give 1×10^4 cells/cm^2 of the well surface and incubated in minimum essential medium (Gibco; Life Technologies, Japan) supplemented without fetal bovine serum. After 2 h incubation at 37 °C in a 5% CO_2 atmosphere, unattached cells were removed by gently rinsing the wells twice with warm phosphate buffered saline (PBS). Attached cells were fixed with 2% paraformaldehyde in PBS. Fluorescent triple staining with DAPI (Nacalai Tesque Japan), monoclonal mouse antivinculin (Sigma-Aldrich Japan), and rabbit anti-FAK[pTyr397] (ENZO Life Scicence USA and Cell Signaling Technology) respectively was used to determine the number of the attached cells and the immunocytochemical localization of vinculin and of the phospholylated focal adhesion kinase in the cells. The secondary antibodies, goat anti-mouse IgG(H+L) (Invitrogen; Life Technologies Japan) and goat anti-rabbit IgG(H+L), were respectively used for the latter two immunofluorescent techniques. The number of attached cells was expressed as the mean value of triplicate determinations. Statistical analyses were performed as follows. Significant difference was evaluated using ANOVA analysis followed by Turkey-Kramer's posthoc test. Data sets were considered as statistically significantly if *p*-values were smaller than 0.05. Peptides P1 and P2 were soluble in water and methanol and therefore could not used to form an insoluble coating, so their ability to *promote* cell adhesion, flattening, and focal adhesions could not be assessed. Instead we assayed the ability 0.2, 0.3, 0.4, and 0.5 mM aqueous solutions of the two peptides to *inhibit* cell adhesion of the same cell line to the untreated surfaces of a 96-well micro plate using the method described above.

8. Alizarin Red Staining for Osteblastic Mineralization. Osteoblastic mineralization was evaluated for plates coated with either *B. mori* silk fibroin or $EAEFN_{10}$ or $SLPF_{10}$. Noncoated wells were used as standard. The MC3T3-E1 cells were added to each well (1×10^4 cells/cm^2) and incubated in minimum essential medium (Gibco) supplemented with fetal bovine serum (MP Biomedicals, USA) at 37 °C in a 5% CO_2 atmosphere. The osteoblastic differentiation-inducing agents, 50 μM ascorbyl-2- phosphoric acid (Sigma-Aldrich Japan) and 10 mM β-glycerophosphoric acid (Nacalai Tesque Japan) were added after 3 day's culture. The osteogenic medium was replaced every 3 days. After 14 and 21 days of incubation, unattached cells were gently rinsed away with two changes of PBS, and the attached cells were then fixed with 2% paraformaldehyde in PBS. Mineralized areas were determined by Alizarin red (Sigma-Aldrich) staining.

RESULTS AND DISCUSSION

1. Conformational Change of Two Peptides Containing TGRGDSPA. The peptides, P1, $E_2(A)_6E_2TGRGDSPA-E_2(A)_6E_2$ and P2, $E_2(A)_{12}E_2TGRGDSPAE_2(A)_{12}E_2$ were soluble in water. We also prepared a similar peptide, $E(A)_{12}ETGRGDSPAE(A)_{12}E$, but its solubility in water was limited, so we were unable to study the effects of the number E residues compared with P2 on the conformation.

We initially used circular dichroism (CD) spectroscopy to study the conformations of P1 and P2. The CD spectrum of P1 showed that at low pH, random coil conformation was strongly predominant with only a low α-helix content (Figure 2A). The helix content, f_H, was estimated from the $[\theta]_M$ value at 222 nm as follows:[31]

$$f_H = -([\theta]_{222} + 2340)/30300$$

As shown in Figure 3A, the helix content was 8% at pH3.8 and approximately zero at pH values ≥ 6.2. In comparison the

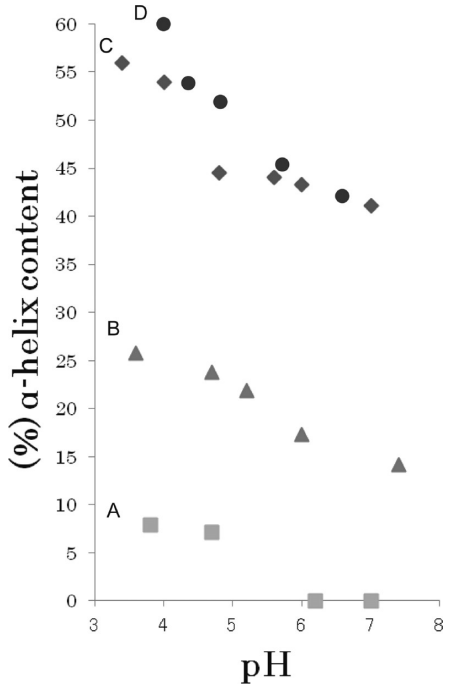

Figure 3. The α-helix content of (A) P1 (■), (B) P2 (▲), (C) $EAEFN_5$ (♦), and (D) $EAEFN_{10}$ (●) determined from the CD spectra recorded at different pH's.

CD pattern of P2 (Figure 2B) gave a helix content of 26% at pH3.6, much higher than in P1. This decreased with increasing pH (Figure 3B). The observation that doubling of the poly(Ala) chain length in P2 compared with P1 led to an increase in α-helical helical content in aqueous solution at low pH is in agreement with the Zim–Bragg helix–coil thermodynamic theory.[32] In addition, as it is known that polyglutamic acids undergoes a coil–helix transition with decreasing pH,[33] the two E_2 residues in P2 are likely to combine with the effect of the longer poly(Ala) chain (n = 12) to enhance the helix formation in acidic condition. This helps to explain the gradual conformational change to random coil with increasing pH in P2 (Figure 2B).

NMR enabled the conformational change induced by an increase in pH to be studied for individual residues[34] in P2. Figure 4 shows changes in the $^{13}C-^{1}H$ HSQC spectra of P2 recorded at pH3.0, pH 5.0, and pH7.0. The ^{1}H and ^{13}C peaks of the Cα(H), Cβ(H) and Cγ (H) groups of the Glu residues shifted gradually as shown by arrows. This is caused by protonation of the COO^- group of the side chain at low pH (pK_a 3.2 for glutamic acid, and 2.0–6.7 for Glu in proteins depending on location[24]). Thus the presence of longer poly(Ala) chains and COO^- group of the Glu side chain in P2 enhance the helix formation at acidic pH condition as observed above. As in the case of the Glu residues, the ^{1}H and ^{13}C peaks (broken arrow) of Asp Cβ(H) groups shift because of the protonation of the COO^- group of the side chain with decreasing pH.

2. The Effect of P1 and P2 on Osteoblast Adhesion. Certain short peptides containing the RGD triplet inhibit cell adhesion by preventing integrin binding and by competing with RGD-containing binding sites on fibronectins.[25] To discover

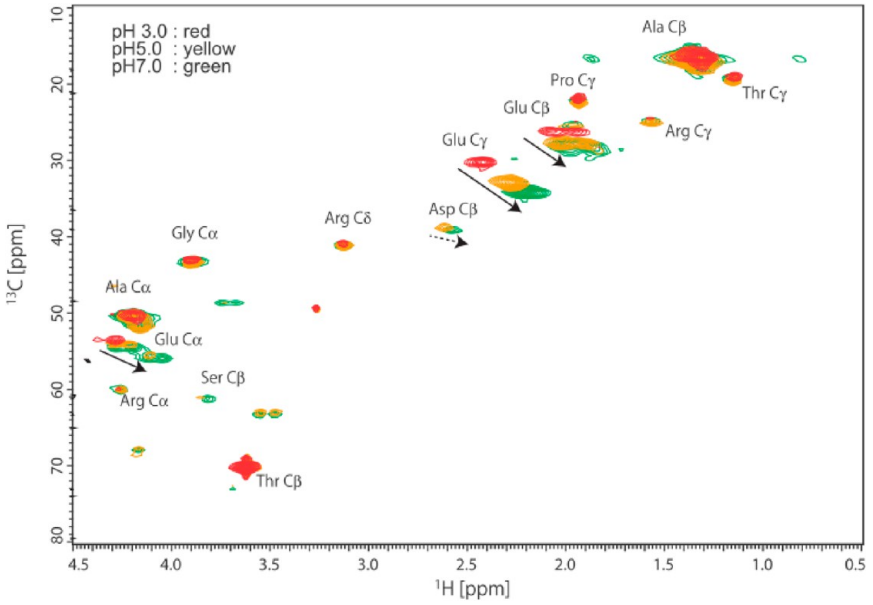

Figure 4. $^{13}C-^{1}H$ HSQC spectra of P2 at different pH's. The assignments are shown.

whether this was true for peptides containing TGRGDSPA and to investigate the effect of poly(Ala) length on osteoblast adhesion to fibronectin, we used synthetic peptides P1 and P2, which differ only in poly(Ala) length (see Materials and Methods and section 1 above). As shown in Figure 5, the addition of 0.2 to 0.3 mM P1 gave a small apparent increase in the cell binding, but this is unlikely to be significant, while 0.4 to 0.5 mM P1 induced a large decrease. For P2, cell adhesion was almost constant at concentrations from 0.2 and 0.4 mM but decreased very strongly between 0.4 and 0.5 mM. This suggests that P1 and P2 may be promising competitive inhibitors of integrin-based MC3T3-E1 cell adhesion to fibronectin and could be used to discover whether cell adhesion is mediated by integrin binding to TGRGDSPA domains in scaffolds containing these domains. We speculate that under the slightly alkaline conditions used, the stronger inhibitory effect of P2 compared with P1may stem from its lower helical and greater random coil contents (see section 1 above) as RGD units in the random coil region may be better exposed and thus able to promote their binding to integrin.

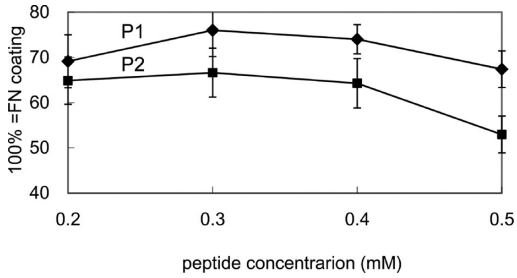

Figure 5. Inhibition by soluble proteins, P1 and P2 of the adhesion of MC3T3-E1 cell fibronectin to untreated plastic (see Materials and Methods section).

3. Conformational Change of EAEFN$_n$ (n = 5, 10). The recombinant protein, EAEFN$_5$ was produced by *E. coli* as described in the Materials and Methods section. The effect of pH values from 3.4 and 7.0 on the CD spectra in aqueous solution is shown in Figure 6. The CD spectrum was dominated by the α-helix pattern, suggesting that the helix content was likely to be considerably greater than in the peptide P2 (Figure 2B). Figure 3C shows that the helix content, f_H, estimated from the CD minimum at 222 nm, $-[\theta]_{222}$, was remarkably high, 56% at pH 3.4 decreasing to 41% at pH 7.0 compared with just 14% at pH 7.4 for P2. Similary, the helix content was determined for EAEFN$_{10}$ as a function of pH. The helix content is almost the same as that of EAEFN$_5$ although the pH dependence is slightly stronger for EAEFN$_{10}$. Thus, the combined effect of the repeated poly(Ala) sequences together with the E_2 units that flank these resulted in a 3-fold increase the helix content compared with P2.

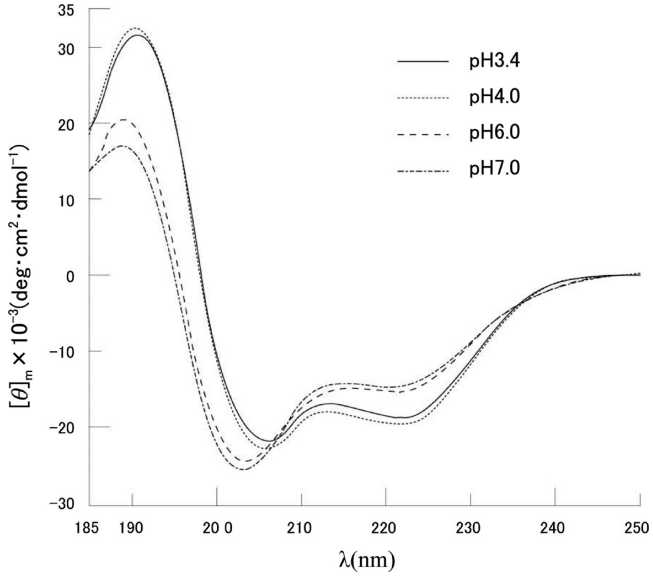

Figure 6. CD spectra of EAEFN$_5$ in aqueous solutions as a function of pH.

The effect of pH change on the poly(Ala) and the RGD domains is seen in $^{13}C-^{1}H$ HSQC NMR spectrum of EAEFN$_5$ recorded at pH 4.0 and 7.0 (Figure 7). The assignments were limited because of additional peaks due to the presence of His-Tag in this protein. However, as in P2, the shifts of the ^{1}H and

dx.doi.org/10.1021/bm401118m | Biomacromolecules 2013, 14, 3731−3741

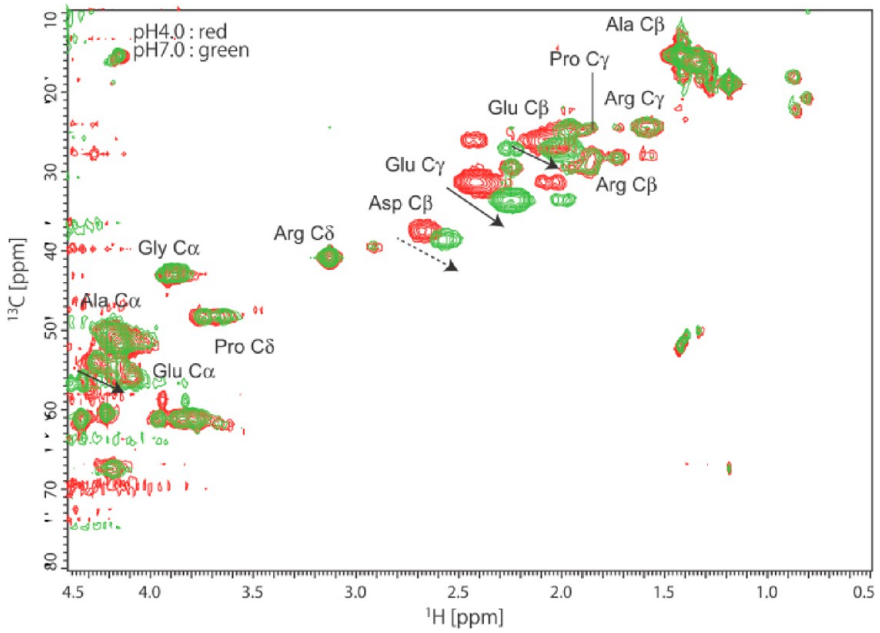

Figure 7. $^{13}C-^{1}H$ HSQC spectra of $EAEFN_5$ in pH = 4.0 and 7.0 together with the assignment.

^{13}C peaks were observed for the Cα(H), Cβ(H) and Cγ (H) groups of the Glu residues of $EAEFN_5$, indicating the protonation of the COO^- group of the side chain with decreasing pH. The difference in helix content in $EAEFN_5$ compared with P2 is illustrated in Figure 8, which superimposes

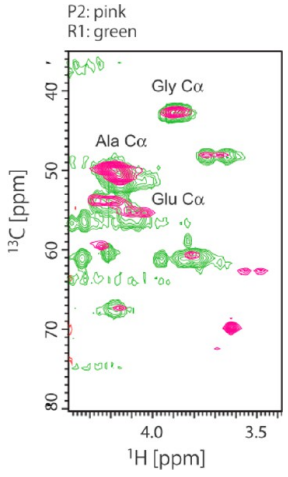

Figure 8. $^{13}C-^{1}H$ HSQC spectra (the expanded Cα region) of P2 and $EAEFN_5$ at pH 7.0.

their $^{13}C-^{1}H$ HSQC spectra of backbone Ala and Glu Cα groups, both recorded at pH 7.0. In general, the backbone Cα peak of polypeptide and protein shifts to higher field by about 2.6 ppm during the random coil to α-helix conformational transition.[17] In this connection, the Cα chemical shift of Ala residue in peptide P2 showed a smaller shift, 50.0 ppm compared with 51.7 ppm in the protein. This is in line with the observation from CD that the helix content of P2 is far smaller than that of $EAEFN_5$ (Figure 3C). In peptide P2, the Glu Cα peak is split into two peaks: one at 55.0 ppm, and the other at 55.2 ppm. In $EAEFN_5$ the upper field peak is at 55.2 ppm, while the lower one is at 56.0 ppm. Thus, in the protein the lower field peak has shifted further (0.8 ppm) than the upper field (0.2 ppm). The splitting of this peak implies that there are two kinds of Glu groups in both P2 and $EAEFN_5$, but there is a larger shift of the lower field peak in the protein. This reflects the much greater helical content of the glutamic acid residues in the protein than in the peptide. This conclusion was supported by the following MD simulation.

4. MD Simulation of $EAEFN_5$. The MD simulation was performed for TS($EAEFN_5$) with the sequence [TS-$[E_2(A)_{12}E_2TGRGDSPAAS]_5$ $]_2$, which has 132 residues. All of the residues in initial structure are assumed to be random coil conformation generated by the Monte Carlo chain growth method as shown in Figure 9A. Even in the random coil state of each residue, a small population, about 10%, will be α-helical, because this represents the lowest energetic state. After MD simulation (Figure 9B), the helix content of the five poly(Ala) regions increased remarkably. Changes in helical content before and after the simulation were plotted for each residue (Figure 9C). After the simulation, the helix content tended to be higher at the center Ala residues of each poly(Ala) domain. The E_2 unit on the N-terminal side of the poly(Ala) domain was also helical, but that on the C-terminal side had a relatively low helical content. This is in agreement with the indication from NMR results that one set of the glutamic acid residues was in a helical conformation at neutral pH while the other was not. A further observation was that the helical content was lower at the sequence, TGRGDSPA.

5. ^{13}C CP/MAS NMR Spectra of $EAEFN_{10}$. Figure 10 shows ^{13}C CP/MAS NMR spectra of freeze-dried $EAEFN_{10}$ samples before and after methanol treatments together with the assignment. This treatment rendered the sample insoluble in water. As shown in Figure 10A, the ^{13}C chemical shifts of the Cα, Cβ and C=O peaks of Ala residues before methanol treatment are 52.5, 15.9, and 176.1 ppm, respectively, indicating that the structure of the PLA domain was α-helical.[17] In this condition, the freeze-dried sample was soluble in water. In contrast, two successive treatments with methanol induced a partial conformation transition as seen ^{13}C CP/MAS the NMR spectrum (Figure 10C) as evidenced by additional Cα, Cβ and C=O carbon peaks of Ala residues respectively at 48.6, 20.0,

dx.doi.org/10.1021/bm401118m | Biomacromolecules 2013, 14, 3731−3741

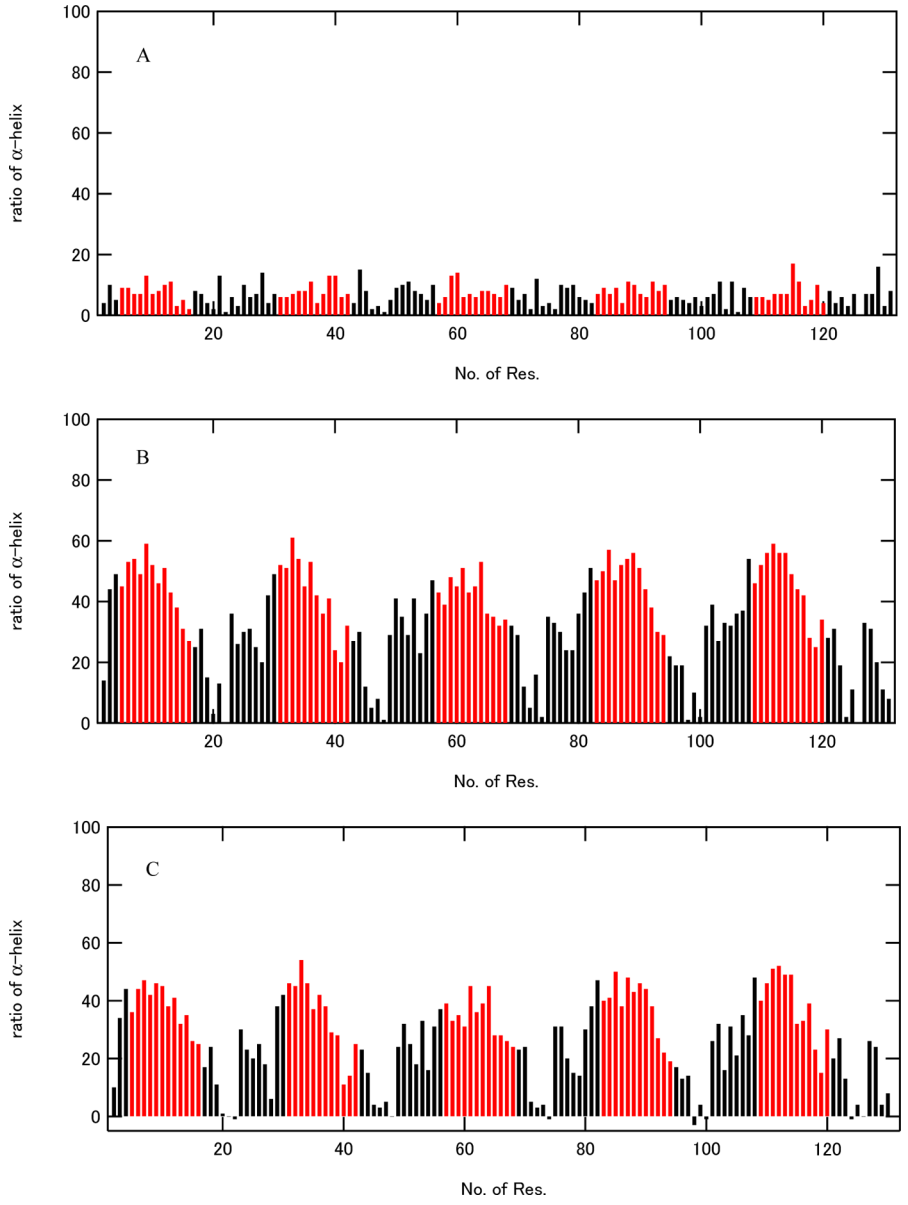

Figure 9. We performed an MD simulation of the conformation in aqueous solution of the protein with the sequence, TSEEAAAAAA[10]AA-AAAAEETG[20]RGDSPAASEE[30]AAAAAAAAAA[40]aa-Eetgrgds[50]PAASEEAAAA[60]AAAAAAAAEE[70]TGRGDSPAAS[80]EEAAAAAAAA[90]AAAAEETG-RG[100]DSPAASEEAA[110]AAAAAAAAAA[120]EETGRGDSPA[130]AS, identical to EAEFN$_5$ but with the addition of the highly hydrophilic N-terminus TS. The α-helix content of each residue against the residue number is shown before and after MD simulations, that is, (A) initial structure, (B) after MD simulation, and (C) the difference B − A. The polyalanine regions are shown in red in the bar graph. The amino acid residues at N and C terminals, T and S, are not shown because the backbone torsion angles are not defined for these terminal residues.

and 171.8 ppm, not seen in the freeze-dried material, indicating structural change from α-helix to β-sheet in the PLA region. By contrast, a single treatment with methanol was insufficient to produce the extent of the of conformation transition seen after two methanol treatments (compare spectra B and C in Figure 10). In this connection, multiple treatments with methanol were necessary to render EAEFN$_{10}$ coatings sufficiently insoluble for use in the osteoblast adhesion study (see below). Thus repeated treatments with methanol are required to produce sufficient structural change to render the material sufficiently insoluble in water. The fraction of β-sheet determined from the Ala peaks after two methanol treatments was estimated to be 30%, an average obtained from deconvolution of the Ala peaks in three spectra including the one illustrated in Figure 10C. In addition, the peaks of other residues, Glu and Gly residues could be observed. The conformation-dependent chemical shift of the Gly Cα carbon is generally small, and for this reason we did not include Gly residues in our analysis. The Glu Cβ chemical shift of the sample without methanol treatment is 26.5 ppm, indicating that Glu residues take α-helix like Ala residue (Figure 10A). The lower field shift of the Glu Cβ peak was observed after two times methanol treatments. Thus structural transition from α-helix to β-sheet also occurs in the Glu residues although it is difficult to monitor the change from the Glu Cα peak because of overlap with other peaks including Ser Cα and Cβ peaks.

6. Cell Adhesion to Surfaces Coated with Either EAEFN$_{10}$ or *B. mori* Fibroin or SLPF$_{10}$. Integrin-binding to RGD-motifs regulates cell adhesion, differentiation, division, and many aspects of cell physiology. The number of MC3T3-

dx.doi.org/10.1021/bm401118m | *Biomacromolecules* 2013, 14, 3731−3741

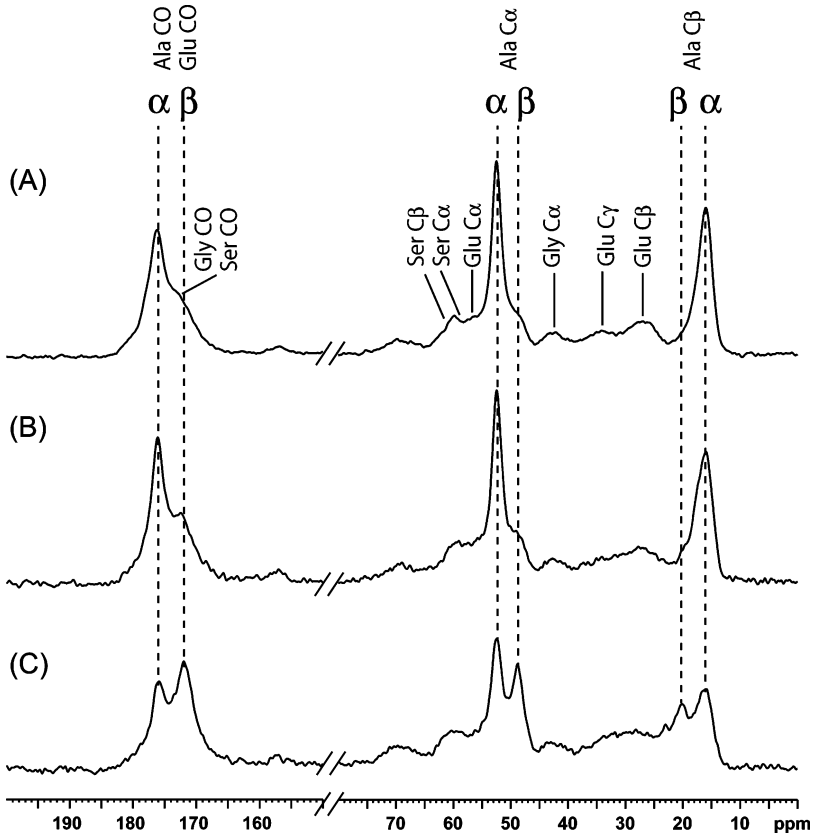

Figure 10. ^{13}C CP/MAS NMR spectra of $EAEFN_{10}$: (A) freeze-dried sample, (B) sample after a single methanol treatment, and (C) sample after two methanol treatments. The peak assignment is also shown in Figure 2A.

E1 cells that remained attached to wells after washing was significantly greater for the $EAEFN_{10}$ coating ($p < 0.05$) than for the uncoated well surface, for wells coated with *B. mori* silk fibroin, and for wells coated with $SLPF_{10}$ (Figure 11A). Enhanced spreading of preosteoblasts was observed on $EAEFN_{10}$ compared with $SLPF_{10}$, *B. mori* silk fibroin, and the uncoated culture well (Figure 11B).

Next we describe the results from immunocytochemical staining of the hemidesmosomal plaque protein vinculin and focal adhesion kinase (FAK) phosphorylation of cells that remain adhering to the above surfaces after 2 h incubation (Figure 11B). One of the first FAK sites phosphorylated upon integrin engagement with fibronectin is the residue Tyr397. FAK phosphorylation generates binding sites for different signaling proteins including Src-family tyrosine and PI3 kinases.[35] In this way, FAK integrates both integrin-stimulated intracellular signaling induced by ECM binding, and growth factor signaling to activate pathways associated with differentiation of osteoblast-like cells. In addition, FAK has been implicated in regulating cell migration and spreading.[35,36] Recent studies suggested that FAK signaling regulates osteogenic differentiation.[37] Additionally, a functional role of fibronectin and its receptor $\alpha_5\beta_1$-integrin in regulating osteogenic differentiation has been demonstrated.[38−42]

Vinculin staining demonstrated the existence of ruffled membranes and numerous focal adhesions in cells bound to the uncoated culture wells or to wells coated with $EAEFN_{10}$ or $SLPF_{10}$. However, both these structures were absent in cells attached to *B. mori* fibroin surfaces on which the cells appeared less flattened and more rounded up. The size of the vinculin-stained focal adhesions appeared largest in the following order $EAEFN_{10}$ = $SLPF_{10}$ > uncoated well, while the number of focal adhesions per unit length of the ruffled membrane appeared similar on $EAEFN_{10}$, $SLPF_{10}$, and the uncoated well. Staining for pFAK and colocalization of this with vinculin was strongest for $EAEFN_{10}$, suggesting that integrin binding had started earlier or progressed further on this substrate compared with the others.

These results suggest that activation of the focal adhesion kinase of MC3T3-E1 cells may occur faster or be more complete on $EAEFN_{10}$ film than on the other surfaces tested. This suggests $EAEFN_{10}$ may enhance adhesion of osteoblast progenitor cells and in so doing stimulate osteoblastic differentiation and that the structure and number of the potential integrin binding sites in this protein may contribute to this.

7. Alizarin Red Staining for Mineral Deposition. Mineralization of the matrix with calcium phosphate can be used as marker for osteogenic differentiation.[43] Figure 12 illustrates the effect of coating the culture wells with $EAEFN_{10}$, or *B. mori* silk fibroin, or $SLPF_{10}$ and of omitting osteogenic medium on mineralization demonstrated by Alizarin staining after 14 and 21 days culture of MC3T3-E1. Although matrix mineralization by cells on surfaces coated $EAEFN_{10}$ and supplemented with osteogenic medium was somewhat less after 14 and 21 days than the uncoated surface, it looks greater at both times than for surfaces coated with *B. mori* silk fibroin or $SLPF_{10}$. Taken together with evidence from our cell adhesion and immunocytochemical staining suggests that cell adhesion of MC3T3-E1 cells via surface integrin to RGD domains on $EAEFN_{10}$ is better at promoting adhesion, osteogenic differentiation, and mineralization than the other

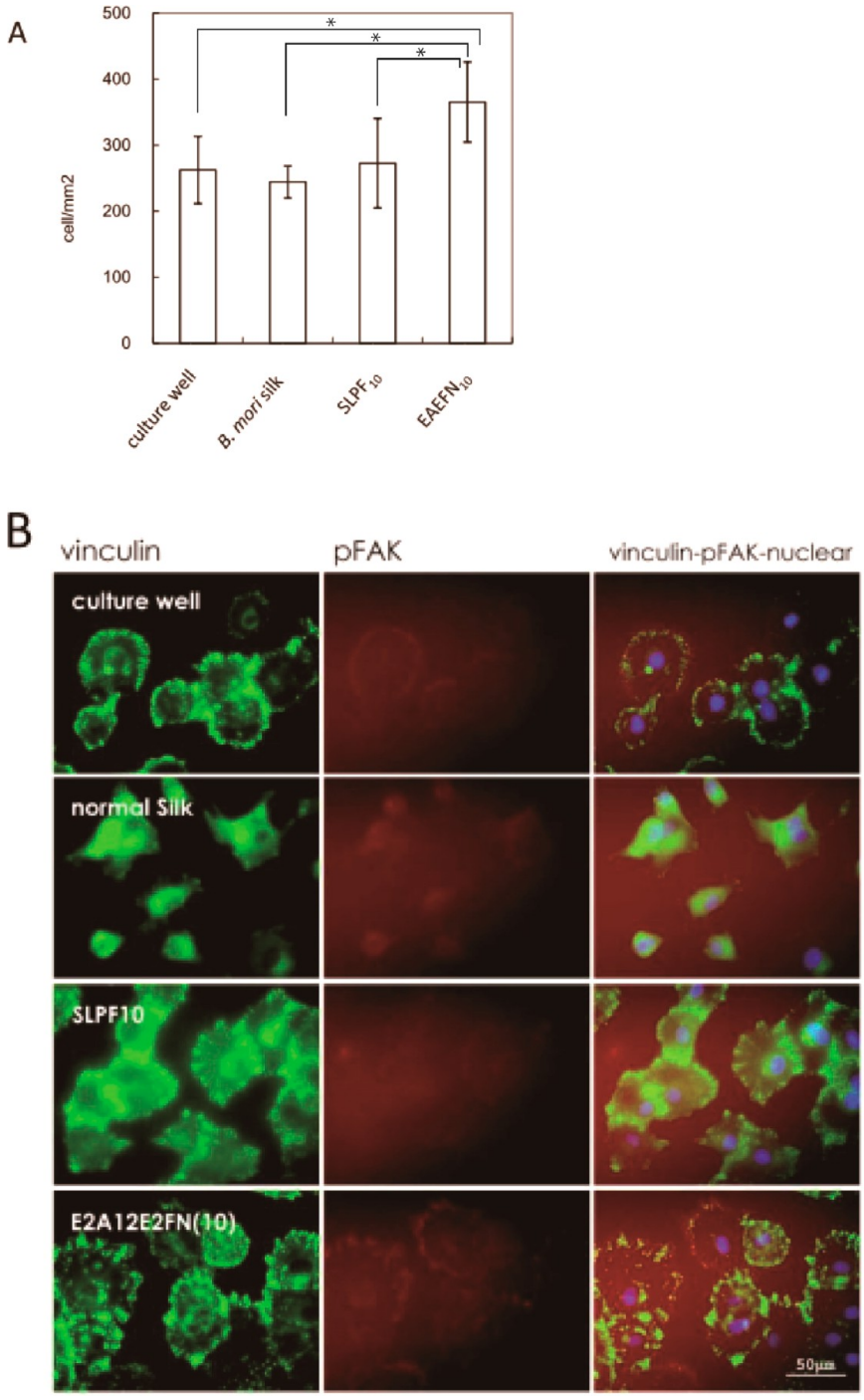

Figure 11. (A) The number of mouse osteoblast-like cell line MC3T3-E1 cells adhering to the surface of uncoated wells or wells coated with either *B. mori* silk fibroin, or $SLPF_{10}$ or after 2 h (see Materials and Methods section). Here the statistical significance symbol * was added ($p < 0.05$). (B) As in panel A, cells stained with DAPI nuclear stain and either an immunostain for vinculin or for phosphorylated focal adhesion kinase (pFAK) (see Materials and Methods section).

two constructs tested. The presence of the EE domains in $EAEFN_{10}$ may facilitate mineralization by providing calcium-binding sites.[22,23]

■ CONCLUSION

We produced a recombinant protein containing poly(Ala), TGRGDSPA, and a pair of E_2 at both the N- and C-terminal sites to render the construct water-soluble and encourage calcium binding. On the basis of results from the appropriate model peptides, we produced the recombinant His tagged protein $EAEFN_5$ by expression in *E. coli*. The solution NMR spectra of the recombinant protein indicated that the poly(Ala) regions were helical, and one E_2 unit was helical, and the other was a random coil. The construct was based on *Antheraea perni* silk fibroin to which cells adhere well. The recombinant protein, $EAEFN_{10}$, was also produced, and after methanol treatment gave a coating that was insoluble in water. Evidence was presented that this coating enhanced both osteoblast adhesion and activated focal adhesion formation, and enhanced osteogenic differentiation compared with the silk fibroin or

dx.doi.org/10.1021/bm401118m | *Biomacromolecules* 2013, 14, 3731−3741

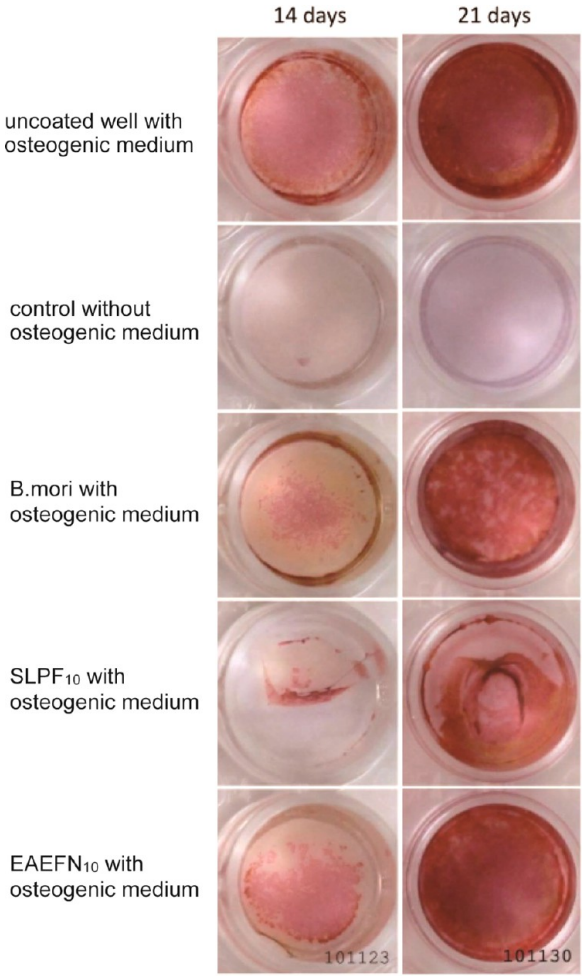

Figure 12. The Arizarin red staining after 14- and 21-day cultures of MC3T3-E1 cells on surfaces coated with either *B. mori* silk fibroin, $SLPF_{10}$, or $EAEFN_{10}$.

two other recombinant proteins containing RGD sequences. Thus we show that the recombinant protein $EAEFN_{10}$ has some of the properties required for a bone tissue engineering scaffold, including insolubility, and evidence of enhanced cell binding through focal adhesions and enhanced osteogenic expression of cells bound to it, and has potential for use as a bone repair material.

AUTHOR INFORMATION

Corresponding Author

*Mailing address: Department of Biotechnology, Tokyo University of Agriculture and Technology, Koganei, Tokyo 184-8588 JAPAN. Fax: (+81) 423837733. E-mail: asakura@cc.tuat.ac.jp.

Notes

The authors declare no competing financial interest.

ACKNOWLEDGMENTS

T.A. acknowledges support from Grant-in-Aid for Scientific Research from the Ministry of Education, Science, Culture and Supports of Japan (23245045) and the Ministry of Agriculture, Forestry, and Fisheries of Japan (Agri-Health Translational Research Project).

REFERENCES

(1) Asakura, T.; Kaplan, D. *Silk Production and Processing*. Academic Press: New York, 1994; p 1.
(2) Kuzuhara, A.; Asakura, T.; Tomoda, R.; Matsunaga, T. *J. Biotechnol.* **1987**, *5*, 199−207.
(3) Demura, M.; Asakura, T. *Biotechnol. Bioeng.* **1989**, *33*, 598−603.
(4) Yoshimizu, H.; Asakura, T. *J. Appl. Polym. Sci.* **1990**, *40*, 127−134.
(5) Demura, M.; Asakura, T. *J. Membr. Sci.* **1991**, *59*, 39−52.
(6) Inouye, K.; Kurokawa, M.; Nishikawa, S.; Tsukada, M. *J. Biochem. Biophys. Methods* **1998**, *37*, 159−164.
(7) Mori, H.; Tsukada, M. *J. Biotechnol.* **2000**, *74*, 95−103.
(8) Sofia, S.; McCarthy, M. B.; Gronowicz, G.; Kaplan, D. L. *J. Biomed. Mater. Res.* **2001**, *54*, 139−148.
(9) Altman, G. H.; Horan, R. L.; Lu, H. H.; Moreau, J.; I, M.; Richmond, J. C.; Kaplan, D. L. *Biomaterials* **2002**, *23*, 4131−4141.
(10) Numata, K.; Kaplan, D. L. *Adv. Drug Delivery Rev.* **2010**, *62*, 1497−1508.
(11) Makaya, K.; Terada, S.; Ohgo, K.; Asakura, T. *J. Biosci. Bioeng.* **2009**, *108*, 68−75.
(12) Demura, M.; Asakura, T.; Kuroo, T. *Biosensors* **1989**, *4*, 361−372.
(13) Sezutsu, H.; Yukuhiro, K. *J. Mol. Evol.* **2000**, *51*, 329−338.
(14) Nakazawa, Y.; Asakura, T. *Macromolecules* **2002**, *35*, 2393−2400.
(15) Minoura, N.; Aiba, S.; Gotoh, Y.; Tsukada, M.; Imai, Y. *J. Biomed. Mater. Res.* **1995**, *29*, 1215−1221.
(16) Minoura, N.; Aiba, S. I.; Higuchi, M.; Gotoh, Y.; Tsukada, M.; Imai, Y. *Biochem. Biophys. Res. Commun.* **1995**, *208*, 511−516.
(17) Nakazawa, Y.; Asakura, T. *Macromolecules* **2002**, *35*, 2393−2400.
(18) Asakura, T.; Tanaka, C.; Yang, M. Y.; Yao, J. M.; Kurokawa, M. *Biomaterials* **2004**, *25*, 617−624.
(19) Tanaka, C.; Asakura, T. *Biomacromolecules* **2009**, *10*, 923−928.
(20) Asakura, T.; Nishi, H.; Nagano, A.; Yoshida, A.; Nakazawa, Y.; Kamiya, M.; Demura, M. *Biomacromolecules* **2011**, *12*, 3910−3916.
(21) Nagano, A.; Kikuchi, Y.; Sato, H.; Nakazawa, Y.; Asakura, T. *Macromolecules* **2009**, *42*, 8950−8958.
(22) Nagano, A.; Sato, H.; Tanioka, Y.; Nakazawa, Y.; Knight, D.; Asakura, T. *Soft Matter* **2012**, *8*, 741−748.
(23) Nagano, A.; Tanioka, Y.; Sakurai, N.; Sezutsu, H.; Kuboyama, N.; Kiba, H.; Tanimoto, Y.; Nishiyama, N.; Asakura, T. *Acta Biomater.* **2011**, *7*, 1192−1201.
(24) Williamson, M. P. *How Proteins Work*; Garland Science/Taylor & Francis: London/New York, 2012.
(25) Tye, C. E.; Rattray, K. R.; Warner, K. J.; Gordon, J. A. R.; Sodek, J.; Hunter, G. K.; Goldberg, H. A. *J. Biol. Chem.* **2003**, *278*, 7949−7955.
(26) Yanagisawa, S.; Zhu, Z. H.; Kobayashi, I.; Uchino, K.; Tamada, Y.; Tamura, T.; Asakura, T. *Biomacromolecules* **2007**, *8*, 3487−3492.
(27) Yang, M.; Tanaka, C.; Yamauchi, K.; Ohgo, K.; Kurokawa, M.; Asakura, T. *J. Biomed. Mater. Res., A* **2008**, *84A*, 353−363.
(28) Delaglio, F.; Grzesiek, S.; Vuister, G. W.; Zhu, G.; Pfeifer, J.; Bax, A. *J. Biomol. NMR* **1995**, *6*, 277−293.
(29) Bascle, J.; Garel, T.; Orland, H.; Velikson, B. *Biopolymers* **1993**, *33*, 1843−1849.
(30) Choi, J. Y.; Lee, B. H.; Song, K. B.; Park, R. W.; Kim, I. S.; Sohn, K. Y.; Jo, J. S.; Ryoo, H. M. *J. Cell Biochem.* **1996**, *61*, 609−618.
(31) Chen, Y. H.; Yang, J. T.; Martinez, H. M. *Biochemistry* **1972**, *11*, 4120−4131.
(32) Zimm, B. H.; Bragg, J. K. *J. Chem. Phys.* **1959**, *31*, 526−531.
(33) Stanley, C. B.; Strey, H. H. *Biophys. J.* **2008**, *94*, 4427−34.
(34) Asakura, T.; Murakami, T. *Macromolecules* **1985**, *18*, 2614−2619.
(35) Sieg, D. J.; Hauck, C. R.; Schlaepfer, D. D. *J. Cell Sci.* **1999**, *112*, 2677−91.
(36) Schwartz, M. A.; Schaller, M. D.; Ginsberg, M. H. *Annu. Rev. Cell Dev. Biol.* **1995**, *11*, 49−99.
(37) Salasznyk, R. M.; Klees, R. F.; Williams, W. A.; Boskey, A.; Plopper, G. E. *Exp. Cell Res.* **2007**, *313*, 22−37.
(38) Moursi, A. M.; Damsky, C. H.; Lull, J.; Zimmerman, D.; Doty, S. B.; Aota, S. *J. Cell Sci.* **1996**, *109*, 1369−80.

(39) Moursi, A. M.; Globus, R. K.; Damsky, C. H. *J. Cell Sci.* **1997**, *110*, 2187−96.
(40) Garcia, A. J.; Vega, M. D.; Boettiger, D. *Mol. Biol. Cell* **1999**, *10*, 785−98.
(41) Keselowsky, B. G.; Collard, D. M.; Garcia, A. J. *Proc. Natl. Acad. Sci. U.S.A.* **2005**, *102*, 5953−7.
(42) Stephansson, S. N.; Byers, B. A.; Garcia, A. J. *Biomaterials* **2002**, *23*, 2527−34.
(43) Gregory, C. A.; Gunn, W. G.; Peister, A.; Prockop, D. J. *Anal. Biochem.* **2004**, *329*, 77−84.